ELSEVIER

Journal of Wind Engineering
and Industrial Aerodynamics 95 (2007) 429–443

JOURNAL OF wind engineering AND industrial aerodynamics

www.elsevier.com/locate/jweia

Nonparametric independent component analysis for detecting pressure fluctuation induced by roof corner vortex

H. He[a,*], D. Ruan[b], K.C. Mehta[a], X. Gilliam[a], F. Wu[c]

[a]*Department of Civil Engineering, Texas Tech University, Lubbock, TX 79409, USA*
[b]*Department of Electrical Engineering and Computer Science, University of Michigan, Ann Arbor, MI 48109, USA*
[c]*Energo Engineering, Houston, TX 77042, USA*

Received 5 October 2005; received in revised form 15 June 2006; accepted 30 August 2006
Available online 19 October 2006

Abstract

The Nonparametric Independent Component Analysis (NICA) method is introduced to detect/infer the presence of roof corner vortex from experimentally measured wind pressure data. Different from the widely recognized Proper Orthogonal Decomposition (POD) method, which decomposes orthogonal pressure modes from the measurement, the NICA method is to separate the statistically independent pressure components/modes from the pressure data. Assuming that the measured wind pressures are caused by mixed wind flow phenomena, this paper attempts to decompose these independent flow induced pressure modes from the measured wind pressure data. Application of the NICA method to wind pressure data collected on the Texas Tech University (TTU) laboratory building justifies that the NICA method successfully separates/extracts from collected wind pressure data the pressure mode that is highly correlated with roof corner vortex. The corresponding time series coefficient of this mode is indicative of the presence of roof corner vortex.

Keywords: Roof corner vortex; NICA; POD; Component; Mode; Time coefficients

*Corresponding author. AIR Worldwide Corporation, 131 Dartmouth Street, Boston, MA 02116, USA. Tel.: +1 734 7546027.
E-mail address: ttuwind@yahoo.com (H. He).

0167-6105/$ - see front matter © 2006 Elsevier Ltd. All rights reserved.
doi:10.1016/j.jweia.2006.08.006

1. Introduction

Wind tunnel tests, full-size experiments, and field damage surveys all revealed the existence of high suctions around roof corners under certain circumstances (Kawai, 2002). Visualization experiments showed that roof corner vortex is a critical factor in producing these high suctions (Fig. 1) and hence extensive roof corner wind damage in reality. In spite of the developing understanding about the pressure-vortex connection, an (semi)-automatic tool remains highly desirable to numerically detect/infer the presence of roof corner vortex from largely existed wind pressure data. Roof corner vortex induced pressure is in nature intermittent and is not necessarily statistically perpendicular to other wind flow induced pressure patterns. This observation casts doubt on the application of widely used Proper Orthogonal Decomposition (POD) approach. On the other hand, it is more reasonable to assume that roof corner vortex is an independent flow phenomenon to other flow phenomena. This paper attempts to introduce a Nonparametric Independent Component Analysis (NICA) framework to detect from the largely existed wind pressure dataset the presence of roof corner vortex induced wind pressure component. This component is conventionally called "wind pressure mode" by wind engineers.

It is not until recent years that researchers began to separate independent wind pressure modes to reflect independent wind flow mechanisms (Gilliam et al., 2004). Before that, efforts were mainly made to decompose wind pressure components from measured wind pressure data by conducting POD analysis (Bienkiewicz et al., 1995) or its variants (Ruan et al., 2005). POD is a statistical tool to decompose the original signal into orthogonal components, and thus enables compression by keeping a few modes where high vibration energies are concentrated. The extracted orthogonal components are independent only if the original data are normally distributed. Since wind pressures exhibit strong non

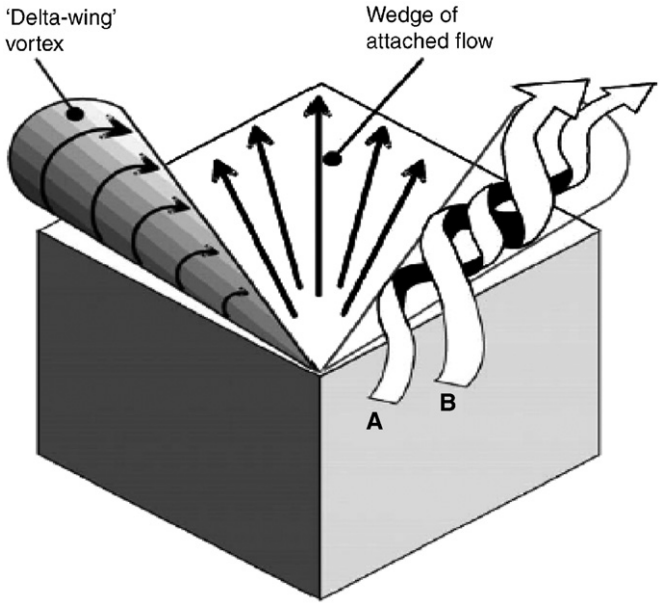

Fig. 1. Roof corner conical (or "Delta-Wing") vortex (by Cook) ICA.

Gaussian properties, POD could not be directly used to identify the independent components underlining the original data. Gilliam et al., (2004) conducted the POD method to a specific set of wind pressure data and found that these wind pressure data can be reduced to a two-dimensional subspace where the perturbation energy is concentrated. An exhaustive search on this subplane is then conducted to find the two coordinates along which the projected wind pressure data approximately exhibit independence. In particular, component dependency was measured by the difference between the joint probability density function and the product of the two marginal probability density functions. This projection pursuit method preceded by POD was tested using Texas Tech University (TTU) data. This approach, however, lacks a rigorous physical interpretation for statistical independence due to POD preprocessing. Because POD and ICA capture very distinct statistical properties of the underlying system (energy concentration vs. statistical independency), the coordinate transforms they carry out can be very different. Thus conducting ICA within the subspace obtained by POD, this approach implicitly assumes the existence of two independent coordinates that coincide with the POD decomposition. This assumption does not hold in general. In addition, projection pursuit approach derived this way is hard to extend to higher dimensions.

In this paper, we introduce a pure independent component analysis approach to separate the pressure component that is highly correlated with roof corner vortex. This approach makes use of Nonparametric Density Estimation (NDE) and is therefore blind to underlying component distributions. The resulting components are totally data-based and truly independent.

2. ICA modeling & objective optimization function

Roof corner vortex has been commonly recognized within wind engineering community as critical wind flows, which could produce high wind pressures. In this paper, NICA was implemented to detect the occurrence of roof conical vortex using the raw wind pressure data collected at TTU's Wind Engineering Research Field Laboratory (WERFL).

Given M samples of wind pressure coefficients for N taps during certain period T, these collected data are arranged in an $N \times M$ matrix with each row of this matrix being the M samples of measured wind pressure coefficients of a tap. This $N \times M$ wind pressure coefficient matrix is denoted as c_{p} and it is assumed to be the output of linear mixing system Ψ whose inputs are unknown independent sources, collectively represented in a. Assuming there are N independent sources, and we can represent the independent source model as

$$c_{\mathrm{p}} = \Psi^* a, \tag{1}$$

where c_{p} (size $N \times M$) is the wind pressure coefficient Matrix (outputs), Ψ (size $N \times N$) is the underlying mixing matrix of the system and a (size $N \times M$) is the component coefficient matrix (source signals).

Our goal is to simultaneously estimate the mixing matrix Ψ and the independent components captured in matrix a. The problem can then be stated as: how to find the pseudo-inverse operator Ω of Ψ (exact inverse when Ψ is invertible), such that when fed with c_p, the inverse system outputs $B = \Omega^* c_p$ will be statistically independent. Herein B is the estimate of a. This problem is typically described in information theory as an optimization problem of finding the best Ω, denoted as Ω_{opt}, so that the mutual

information between the reconstructed wind pressure components $(b1, b2, \cdots b_N)$ is minimized (Roberts and Everson, 2001; Bell and Sejnowski, 1995):

$$\Omega_{\text{opt}} = \arg\min_{\Omega} I(b1, b2, \cdots b_N) \tag{2}$$

with $b1$, $b2, \ldots$, b_N being the rows of $B = \Omega^* c_p$.

Using the definition of mutual information, the optimization formula (2) can be written as (Cover and Thomas, 1991)

$$\arg\min_{\Omega}\left\{\sum_{i=1}^{N} H(b_i) - \log|\det\Omega| - H(a)\right\}, \tag{3}$$

where the entropy $H(a)$ is a constant independent of Ω, thus it is equivalent to minimize the following objective function:

$$L(\Omega) = \sum_{i=1}^{N} H(b_i) - \log|\det\Omega| = -\sum_{i=1}^{N} E\left[\log p_{bi}(\Omega_i a)\right] - \log|\det\Omega|, \tag{4}$$

where Ω_i is the ith row of the matrix Ω.

3. Expansion of optimization function through NDE

Unlike the regular ICA approach, NICA is totally blind to the underlying structures of wind pressure components. It makes no presumption on the statistical distributions of wind pressure components.

We use a nonparametric model to estimate the density function P_{b_i}. Given the observation, the marginal distribution of a reconstructed source is approximated as

$$p_{b_i}(b_i) = \frac{1}{Mh}\sum_{m=1}^{M}\phi\left(\frac{b_i - B_{im}}{h}\right),\ i = 1, 2, ..., N, \tag{5}$$

where ϕ is the Gaussian kernel function $\phi(u) = \frac{1}{\sqrt{2\pi}}e^{-u^2/2}$, h is the selected kernel bandwidth, B_{im}'s are the kernel centroids $B_{im} = \Omega_i c_p^{(m)} = \sum_{n=1}^{N}\omega_{in}c_{p_{nm}}$, where $c_p^{(m)}$ refers to the mth column of c_{p} and ω_{in} is the element (the ith row and the nth column) of Ω or the nth element or vector Ω_i.

By substituting definition of b_i and B_{im} into (5), we get

$$p_{b_i}\left(\Omega_i a^{(k)}\right) = \frac{1}{Mh}\sum_{m=1}^{M}\phi\left(\frac{\Omega_i\left(a^{(k)} - a^{(m)}\right)}{h}\right). \tag{6}$$

By inserting Formula (6) to Formula (4), the objective optimization function in Formula (4) can then be written as

$$\begin{aligned} L(\Omega) &= -\frac{1}{M}\sum_{i=1}^{N}\sum_{k=1}^{M}\log\left[\frac{1}{Mh}\sum_{m=1}^{M}\phi\left(\frac{\Omega_i\left(c_p^{(k)} - c_p^{(m)}\right)}{h}\right)\right] - \log|\det\Omega|, \\ &= -L_0(\Omega) - \log|\det\Omega|. \end{aligned} \tag{7}$$

Our problem can then be expressed as

$$\Omega_{\text{opt}} = \arg\min_{\Omega} L(\Omega)\ \ s.t.\|\Omega_i\| = 1,\ \ i = 1, ..., N, \tag{8}$$

where $\|\Omega_i\|$ is the L2-norm of vector Ω_i. The additional constraint $\|\Omega_i\| = 1,\ \ i = 1, ..., N$ is for restricting the resulting Ω_{opt} to a finite set. By this constraint, the other matrices rescaled or permuted from the resulting Ω_{opt} can be excluded.

4. Optimization algorithm of NICA

To simplify notation, we define as in (Boscolo and Pan, 2004) the following quantity:

$$Z_i(k,m) = \frac{\Omega_i\left(c_p^{(k)} - c_p^{(m)}\right)}{h} = \frac{1}{h}\sum_{j=1}^{N} \omega_{ij}\left(c_{pjk} - c_{pjm}\right). \tag{9}$$

We also incorporate the unity constraint on the norm of Ω_i by a normalization transformation as

$$\Omega_i = \frac{\tilde{\Omega}_i}{\|\tilde{\Omega}_i\|},\ \ i = 1, ..., N. \tag{10}$$

Accordingly, we define $\tilde{Z}$ via

$$\tilde{Z}_i(k,m) = \frac{\tilde{\Omega}_i\left(c_p^{(k)} - c_p^{(m)}\right)}{h} = \frac{1}{h}\sum_{j=1}^{N} \tilde{\omega}_{ij}\left(c_{pjk} - c_{pjm}\right). \tag{11}$$

Provably, the derivative of the second item $\log|\det \Omega|$ in Formula (7) with respect to $\tilde{\omega}_{ij}$ constantly equals zero for all i, j pairs. Therefore the derivative of the objective function with respect to $\tilde{\omega}_{ij}$ becomes

$$\frac{\partial L_0(\tilde{\Omega})}{\partial \tilde{\omega}_{ij}} = \frac{1}{M}\sum_{k=1}^{M} \frac{\sum_{m=1}^{M} \frac{\partial \tilde{Z}_i(k,m)}{\partial \tilde{\omega}_{ij}} \phi'\left[\tilde{Z}_i(k,m)\right]}{\sum_{m=1}^{M} \phi\left[\tilde{Z}_i(k,m)\right]}, \tag{12}$$

where

$$\frac{\partial \tilde{Z}_i(k,m)}{\partial \tilde{\omega}_{ij}} = \frac{1}{h}\left(c_{pjk} - c_{pjm} - \tilde{Z}_i(k,m)\tilde{\omega}_{ij}\right),$$

$$\phi'\left[\tilde{Z}_i(k,m)\right] = -\tilde{Z}_i(k,m)\phi\left[\tilde{Z}_i(k,m)\right].$$

At this point, we are free to choose any gradient descent algorithm to solve the optimization problem (Bertsekas, 1999). Many standard toolboxes are available for solving such standard unconstrained (the original constraint has been enforced by the transformation as Formula (10)) optimization problem. We use the built-in Quasi–Newton (QN) method with MATLAB software (The Mathworks, Natick, MA) in our implementation.

5. Experimental setup

To observe the roof corner conical vortex phenomenon, a field experiment was conducted at the TTU WERFL building (Levitan and Mehta, 1992a, b). This experiment

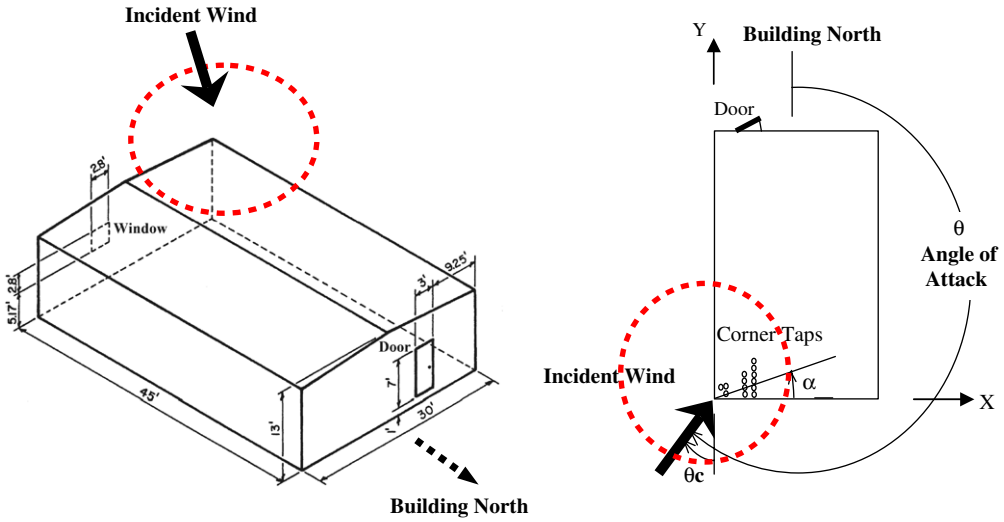

Fig. 2. Illustrations of experimental layout and terminology.

was composed of two parts: a regular wind speed and wind pressure measuring system, and a flow visualization and synchronized data acquisition system.

The TTU WERFL building is 13.7 m × 9.1 m × 4.0 m (length × width × height) in size. A total of 25 taps were distributed around the roof corner area (3 m × 3 m) for measuring conical vortex induced wind pressures (Fig. 2). Taps were numbered following the convention described in (Levitan and Mehta, 1992a, b). For precision, two sonic anemometers were installed, one on the corner of the roof and the other right above the roof surface and close to the tuft-grid frame.

The tuft-grid method was used to capture the highly turbulent wind flow on the roof corner. Yarn strands with a length of 0.18 m were used as tufts to visually display the wind flow. As shown in Fig. 3, these yarn strands were tied at the nodes of a 2.13 m × 0.12 m tuft-grid frame with 0.1 m spaced grids. The tuft-grid frame was set perpendicular to the short roof edge and close to the corner. An 8 mm video camera was set perpendicular to the frame and facing the wind so that the visualized wind flow can be recorded.

Synchronizing the video, wind, and pressure data collecting is a critical task in this experiment. The light emission diode (LED) method was used in this experiment. The LED voltage signal is recorded by the video as well as wind and pressure data so that it can be taken as a reference system to synchronize video images, wind data, and pressure data. Details of this method can be found in (Letchford, 1995; Zhao, 1997; Banks et al., 2000; Wu, 2000).

6. Vortex induced pressure component separation

The data of Run test M52R111 are used to test the proposed blind separation method. M52R111 represents the Run 111 test with the Mode 52 experimental setup. Fig. 4 shows the distribution of taps on the roof corner for Mode 52. In total, 25 taps are distributed on a 3 m × 3 m square area on the roof corner. Validated wind pressure data are collected for

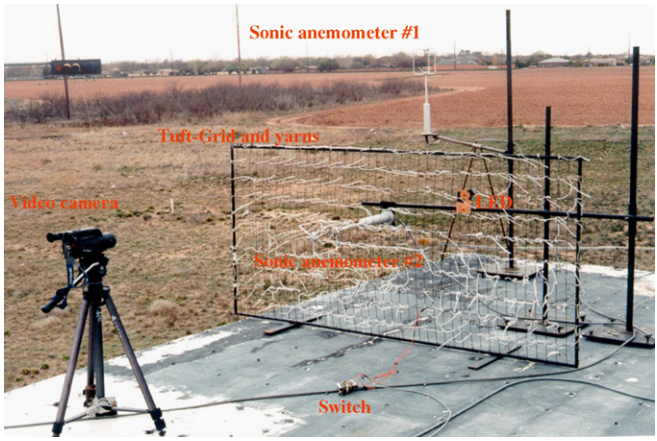

Fig. 3. Picture of flow-visualization experimental setup.

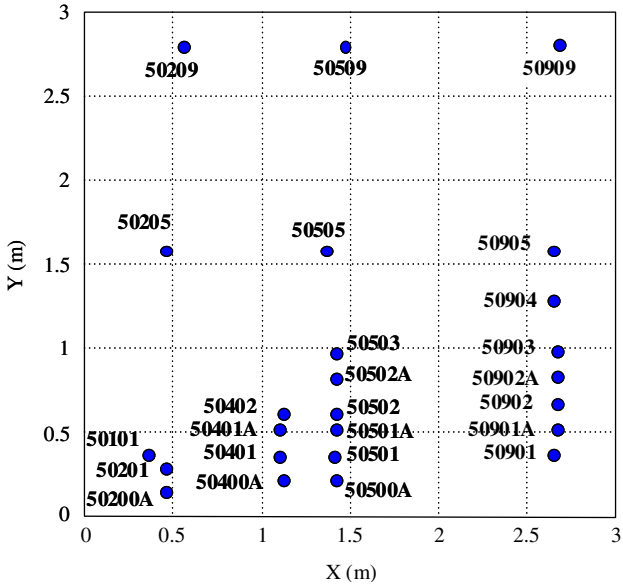

Fig. 4. Roof corner tap distribution.

23 of them. Wind speeds at different heights (8, 13, 33, 70 and 160 ft) are measured by wind-speed anemometers mounted on a 160-ft high meteorological tower.

Roof corner pressures are measured at a frequency of 30 Hz for 900 s, resulting in a time series record of 27000 values for each tap. Wind speeds and directions are measured at 10 Hz for 900 s with 9000 values recorded for each testing run.

In total, 23 independent components can be obtained using the presented blind separation method. It is noteworthy that due to complex and mixed natures of the wind pressure data there are 23 independent components without obvious dominating

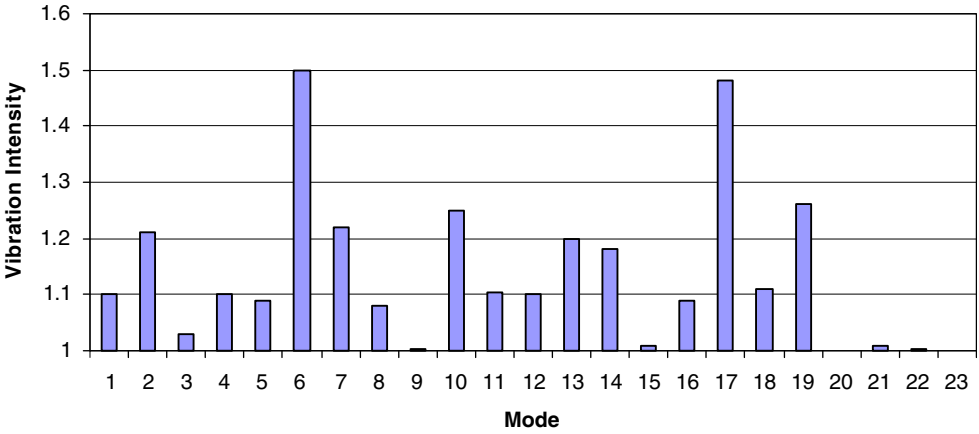

Fig. 5. Vibration intensities of independent modes of wind pressure data.

ones. Fig. 5 shows the root mean squared (RMS) values of the temporal coefficients for each component. RMS is a good indicator of vibrating energy for these components.

It can be noted from Fig. 5 that Mode 6 and Mode 17 have greater vibrating energies than the other components. Since the visual observation of airflow during Run 111 revealed strong intermittent roof corner vortices, it is reasonable to expect that either Component 6 or Component 17 be highly correlated with roof corner vortex. Modes 6 and 7, along with their corresponding time coefficients, are shown in Figs. 6–9. Close examination of time coefficients of component 6 and component 17 reveals that component 6 is highly correlated to roof corner vortex. It can be noted in Fig. 7 that component 6 is weak at Time 1 and Time 3. Consistently, no roof corner vortex was seen at Time 1 and Time 3 in Fig. 10. Likewise, component 6 is strong at Time 2 and Time 4 in Fig. 7 and meanwhile roof corner vortices were observed in Fig. 10. The observed correspondence between Figs. 7 and 10 indicates that component 6 is highly correlated to roof corner vortex induced pressure mode. It is noteworthy that the intermittent roof corner vortex induced pressure mode, if present, varies spaciously with time. The pressure mode shown in Fig. 6 is highly correlated to the roof corner vortex induced pressure mode yet it is not the roof corner vortex induced pressure mode.

Different from Mode 6, Mode 17 seems to reflect a mixture of the conical vortex induced pressure mode and the large-scale wake induced pressure mode. Close examination of Figs. 9 and 10 reveals no correlation between Mode 17 and roof corner vortex.

As argued in the introduction section, roof pressures are caused by various mixing wind flow phenomena, which are nonorthogonal to each other. Hence the POD method, which separates independent pressure modes, seems to be improper for detecting roof vortex. This judgment is tested numerically. Fig. 11 shows the pressure Mode 1 by POD analysis. Fig. 12 plots the corresponding time coefficients of this mode. The comparison of Fig. 12 with Fig. 10 shows certain level of correlation. However, this correlation does not always hold well. For example, coefficients of Mode 1 by POD at Time 4 are close to zero while from Fig. 10 we know there was obvious corner vortex at Time 4.

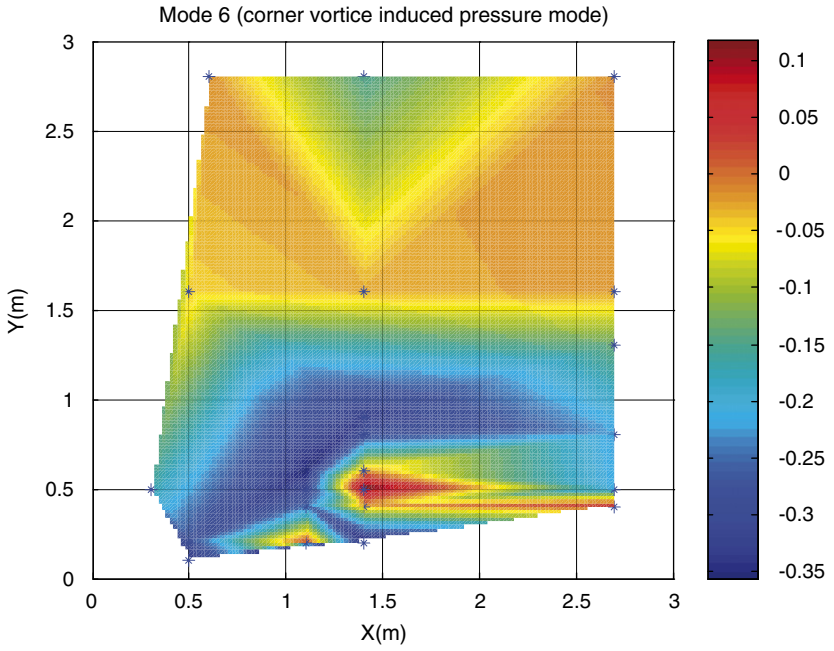

Fig. 6. Mode 6 by NICA.

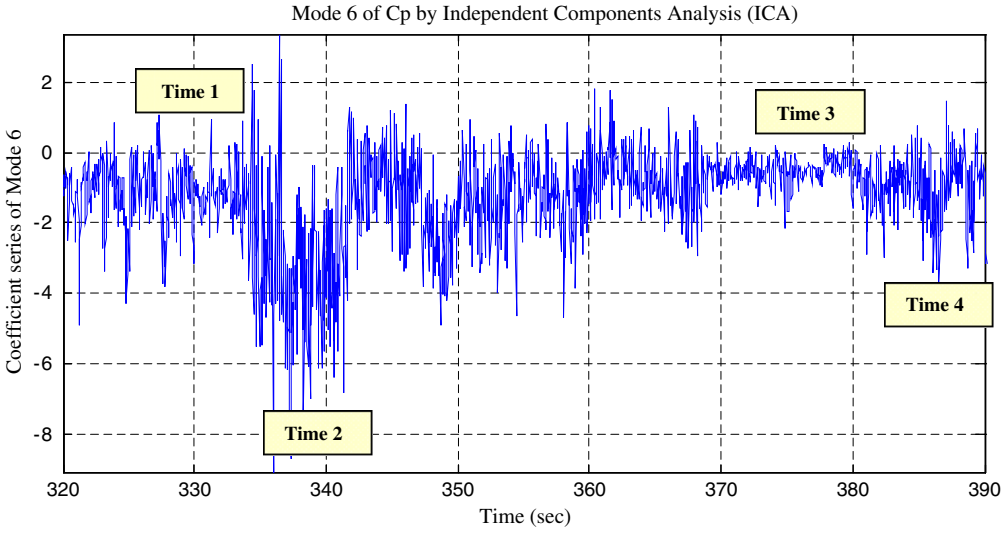

Fig. 7. Coefficients of Mode 6 by NICA.

By plotting the time series of the horizontal angles of attack of Test M52R111, it can be seen from Fig. 13 that during Time 2 and Time 4 the angles of attack are around 210–220°, while during Time 1 and Time 3 the angles of attack are far from this range. This observation, along with the observation that corner vortices happened at Time 2 and Time 4 while they did not happen at Time 1 and Time 3, could easily result in the same

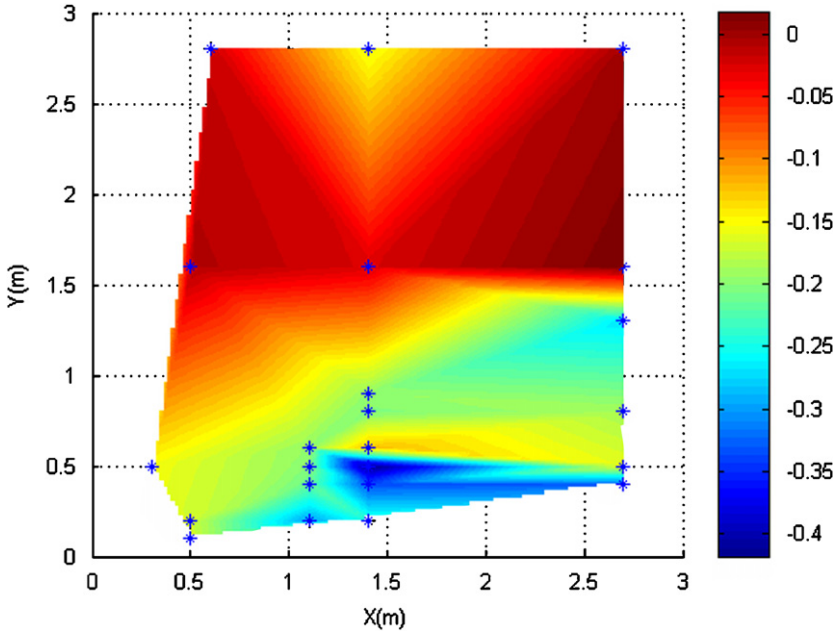

Fig. 8. Mode 17 by NICA.

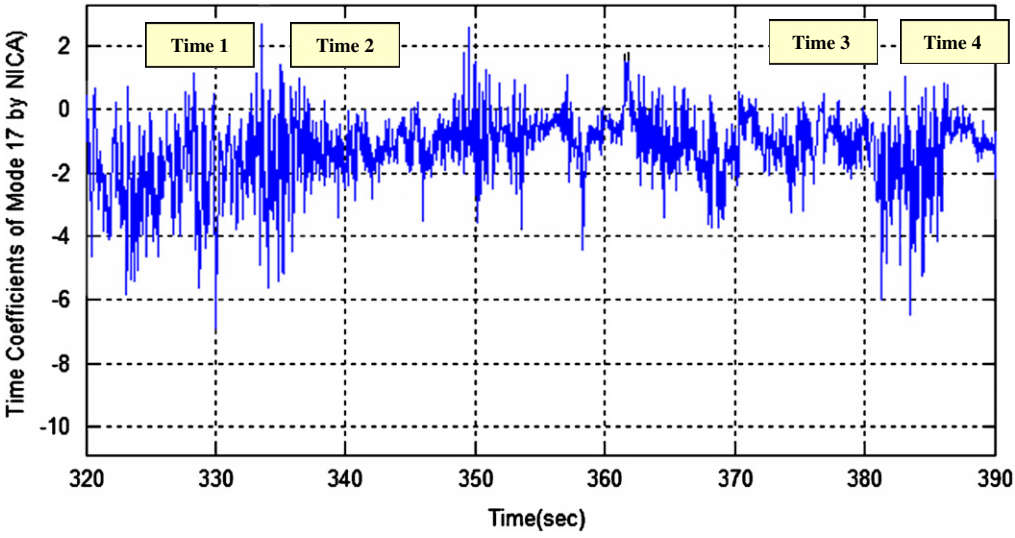

Fig. 9. Coefficients of Mode 17 by NICA.

conclusion as (Wu et al., 2001), which claims that corner vortices tend to occur when the horizontal angle of attack is around 210–220° (Figs. 14 and 15).

It can be noted from Fig. 7 that the intensity of component 6 during Time 4 is obviously weaker than that during Time 2. This difference can be mainly attributed to the upcoming wind speed difference during the two time segments. Although Time 2 and Time 4 both

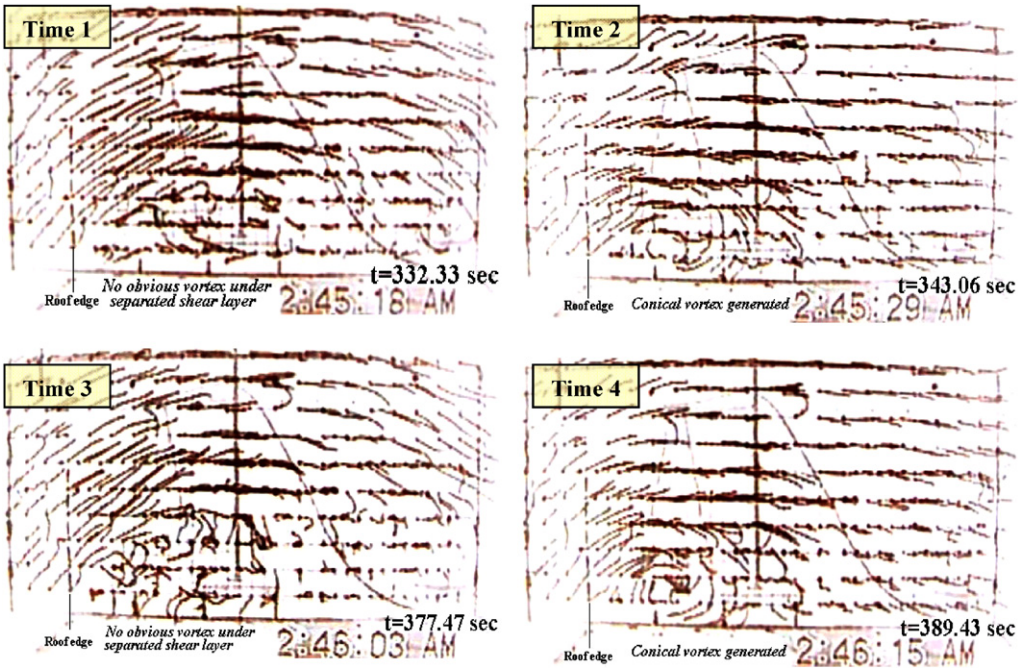

Fig. 10. Images of the recorded flow at the four time points.

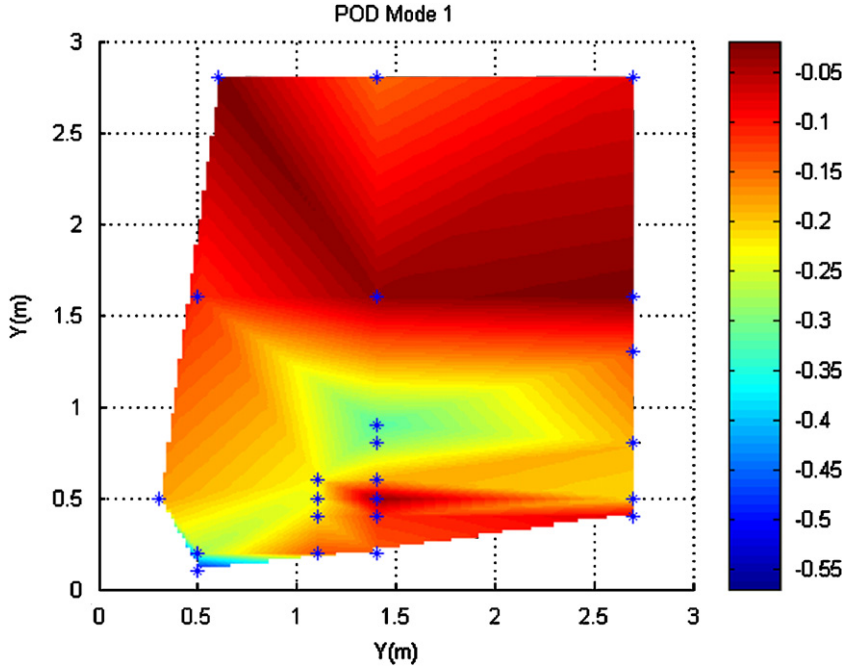

Fig. 11. Mode 1 by POD.

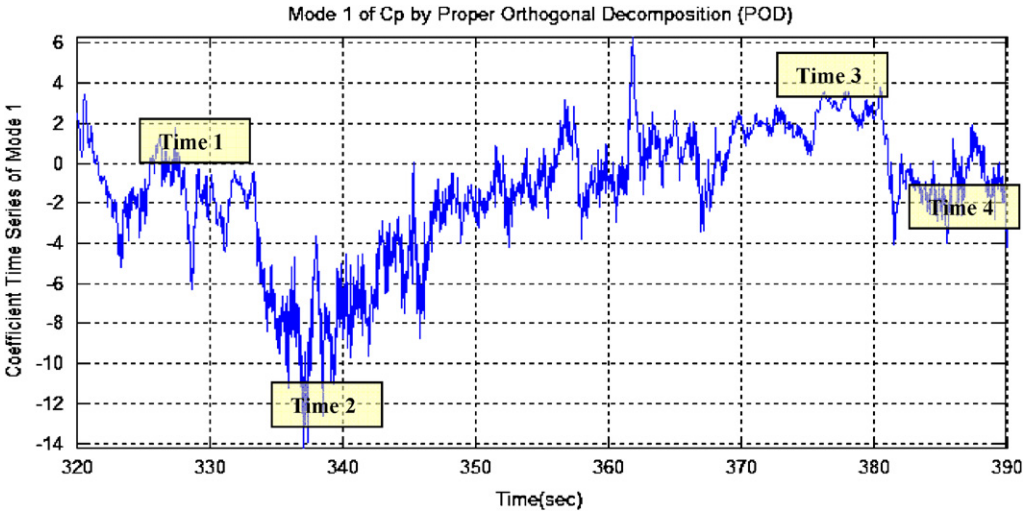

Fig. 12. Coefficients of Mode 1 by POD.

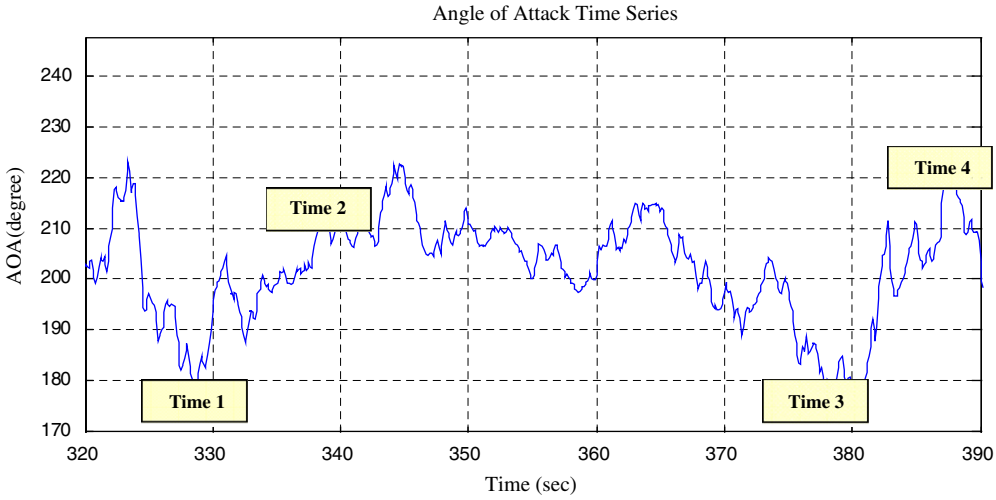

Fig. 13. Time series of angle of attack (AOA).

experienced roof corner vortices, it is reasonable to expect that vortices during Time 4 are weaker than vortices during Time 2 due to the fact that wind speeds during Time 4 are much lower than wind speeds during Time 2 (Fig. 14).

As claimed by Wu et al. (2001), the phenomenon of roof corner vortices is a major mechanism that causes high suction on roof corner areas. This claim can be justified in our case by Fig. 15, where strong simultaneity can be noted between temporal coefficients of Component 6 and pressure coefficients of three typical taps. The existing but weaker simultaneous relationship between the pressure coefficients at Tap 50902A and the

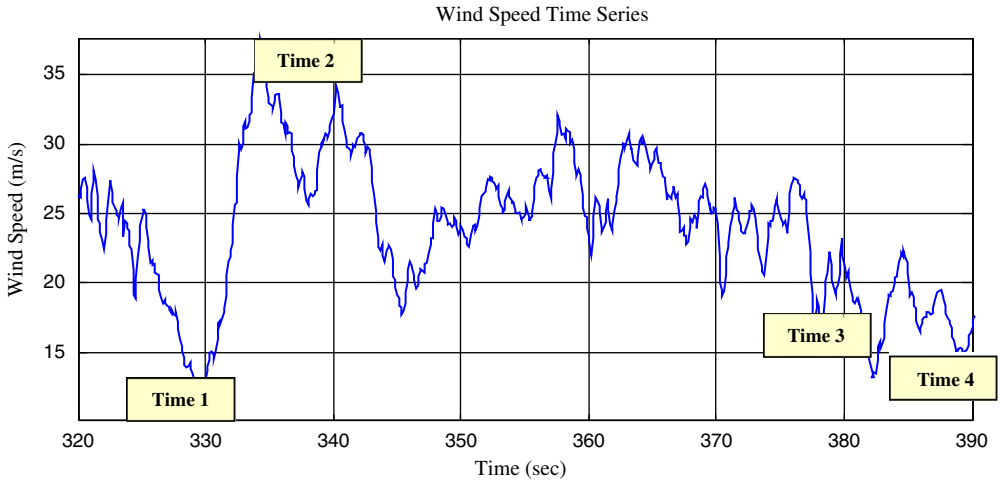

Fig. 14. Time series of upcoming wind speeds.

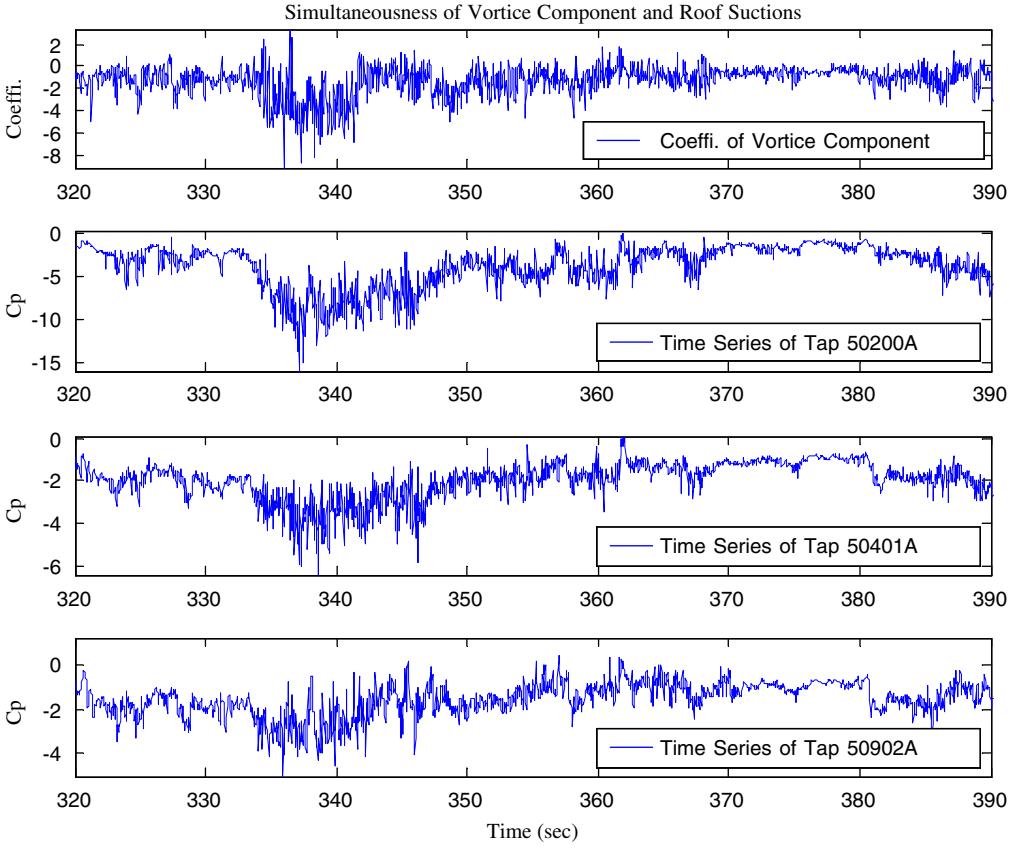

Fig. 15. Illustration of the effects of corner vortices on suction pressures.

temporal coefficients of Component 6 can be attributed to the location of this tap. Tap 50902A, compared with Tap 50200A and Tap 50401A, is located farther from the roof corner and is expected to take less influence from roof corner vortices.

7. Concluding remarks

This work attempts to detect the presence of roof corner vortices from the original measured wind pressure data. The NICA method is introduced for this purpose. No presumption is made in this nonparametric method regarding the statistical distribution of components underlying the original data. This assures that the method is totally data-based. In contrast to the previous mixed approach of POD and projection pursuit (Gilliam et al., 2004), NICA results in totally independent wind pressure modes. In addition, NICA theoretically can be applied to any high dimension decomposition/analysis.

Experimental computations indicate that the NICA method can be used to detect the presence of roof corner vortex induced pressures from measured wind pressure data. Strong correlation is observed between time coefficients of a particular pressure mode decomposed by the NICA method and the simultaneous flow visual records. The temporal coefficients of the roof corner vortices induced pressure component are highly indicative of the occurrence and strength of roof corner vortices. In addition, the corner vortices are observed, as expected, to occur under the condition that the horizontal angle of attack is around 210–220°.

Given the developing understanding about the pressure-vortex connection from experimental observations and by theoretical inferences, an (semi)-automatic way to numerically detect/infer the presence of vortex is still desirable. Detection of roof corner vortex by visible observation of wind flow videos is both expensive and unreliable due to inter-observer difference and subjectivity. Perfect synchronization is also a potential issue. The proposed method offers a potential tool to detect/infer roof vortex from large wind pressure database. Large amount of such analysis results may provide some guidance regarding the nurturing conditions of roof vortex.

References

Banks, D., Meroney, R.N., Sarkar, P.P., Zhao, Z., Wu, F., 2000. Flow visualization of conical vortices on flat roofs with simultaneous surface pressure measurement. J. Wind Eng. Ind. Aerodyn. 84 (1), 65–85.

Bell, A.J., Sejnowski, T.J., 1995. An information-maximizatin approach to blind separation and blind deconvolution. Neural Comput. 7 (6), 1129–1159.

Bertsekas, D.P., 1999. Nonlinear Programming, second ed. Athena Scientific.

Bienkiewicz, B., Tamura, Y., Ham, H.J., Ueda, H., Hibi, K., 1995. Proper orthogonal decomposition and reconstruction of multi-channel roof pressure. J. Wind Eng. Ind. Aerodyn. 54-55, 369–381.

Boscolo, R., Pan, H., 2004. Independent component analysis based on nonparametric density estimation. IEEE Trans. Neural Networks 15 (1), 55–65.

Cover, T.M., Thomas, J.A., 1991. Elements of Information Theory. Wiley, New York.

Gilliam, X., Dunyak, J.P., Smith, D.A., Wu, F., 2004. Using projection pursuit and proper orthogonal decomposition to identify independent flow mechanisms. J. Wind Eng. Ind. Aerodyn. 92 (1), 53–69.

Kawai, H., 2002. Local peak pressure and conical vortex on building. J. Wind Eng. Ind. Aerodyn. 90 (4–5), 251–263.

Letchford, C.W., 1995. Simultaneous flow visualization and pressure measurements on the Texas Tech building. In: Proceedings of the Ninth International Conference on Wind Engineering, New Delhi, India.

Levitan, M.L., Mehta, K.C., 1992a. Texas tech field experiments for wind loads part I: building and pressure measuring system. J. Wind Eng. Ind. Aerodyn. 41–44, 1565–1576.

Levitan, M.L., Mehta, K.C., 1992b. Texas tech field experiments for wind loads part II: meteorological instrumentation and terrain parameters. J. Wind Eng. Ind. Aerodyn. 41–44, 1577–1588.

Roberts, S., Everson, R., 2001. Independent Component Analysis: Principles and Practice. Cambridge Press, Cambridge.

Ruan, D., He, H., Castañón, D.A., Mehta, K.C., 2005. Normalized proper orthogonal decomposition (NPOD) for building pressure data compression. J. Wind Eng. Ind. Aerodyn. 94/6, 447–461.

Wu, F., Sarkar, P.P., Mehta, K.C., 2001. Full-scale study of conical vortices and roof corner pressures. Wind Struct. 4 (2), 131–146.

Wu, F., 2000. Full-scale study of conical vortices and their effects near roof corners. Ph.D. Dissertation, Texas Tech University, Lubbock, TX.

Zhao, Z., 1997. Wind flow characteristics and their effects on low-rise buildings. Ph.D. Dissertation, Texas Tech University, Lubbock, TX.